On the Effect of Vibrating Targets in Bistatic SAR Images

Carmine Clemente, John J. Soraghan
Centre of Excellence for Image and Signal Processing, University of Strathclyde, Glasgow, U.K
carmine.clemente@eee.strath.ac.uk

***Abstract*—Bistatic Synthetic Aperture Radar (BSAR) provides strategical, technical and economical advantages in radar imaging. Motions and micro-motions of objects in an illuminated scene introduces Doppler and micro-Doppler effects in the received radar echoes. This paper investigates the result on a focussed image due to a vibrating target in a bistatic SAR. The results are shown to be different from the monostatic case. The paper analyses this effect mathematically and simulations results show that the output from the derived model are critically dependent on the acquisition geometry of the Bistatic SAR system.**

***Index Terms*—Bistatic SAR, micro-Doppler effect.**

I. Introduction

Bistatic SAR operates with a separate transmitter and receiver introducing new characteristics compared to traditional monostatic SAR systems [1]. Some of the advantages of the bistatic configuration include i) the reduction of vulnerability of the system in military applications with the ability of having the transmitter located at a safe distance from the hostile area ii) the capability for the bistatic system to be employed for imaging in the flight direction or backwards in flight assistance systems iii) reduction of costs iv) measurement of the bistatic clutter characteristic and v) the reduction of the dihedral and polyhedral effects in urban areas improving the image's quality. These advantages encouraged the remote sensing community to investigate new bistatic experiments with differents configurations [2]–[7] that provided interesting results in terms of resolution and target detection. In [8] the micro-Doppler signature for vibrating targets in a monostatic SAR system was analyzed and tested with an X-band radar, while in [9] the micro-Doppler for vibrating and rotating SAR was analyzed and tested with a millimeter Wave (mmW) radar. In both cases time-frequency analysis was performed using the Wigner Ville Distribution exploiting the properties of the Cohen'transforms [10].

In this paper the effects introduced by the micro-motion of targets in bistatic SAR systems is investigated theoretically and shown to be particularly dependent on the Bistatic acquisition geometry. This is due to the fact that the induced micro Doppler is dependent on the geometry. It is shown that the received signal model for a vibrating target can be expanded in a series of Bessel functions. However unlike the monostatic case the argument of the Bessel functions is seen to be dependent on the acquisition geometry in a Bistatic SAR system. In the paper a model for this dependence will be mathematically derived and analyzed through simulations highlighting the effect of different configurations observed from the same vibrating target. The results show that the same vibration exhibits a different number of visible ghost scatterers with different amplitudes for different configurations. This demonstrates the importance of the knowledge of the bistatic geometry in bistatic SAR image interpretation in order to make effective use of the extracted micro Doppler signatures. The remainder of paper is organized as follows. In section II the bistatic SAR geometry and the received signal model are discussed. In section III the micro-Doppler effect from a vibrating target in the bistatic geometry is introduced and analyzed as the effect on the focussed image of the bistatic geometry. Section IV presents simulation results of focussed vibrating target. Section V concludes the paper.

II. Fixed Receiver Bistatic SAR Geometry

In a bistatic SAR the transmitter and the receiver can have different velocities, altitudes and flight paths, leading to the possibility of having different acquisition configurations. The simplest case is when both transmitter and receiver have the same velocity and parallel flight paths, while a more complicated configuration exists when the platforms have different velocities and non parallel flight paths. In the case of a fixed receiver configuration, only the transmitter is moving and the receiver is fixed. This configuration allows existing monostatic SAR missions to be exploited [7], in addition the focussing step is easier, permitting an easier and cheaper test bench to validate new techniques to be extended in the more general bistatic configurations. For these reasons we choose to perform the first analysis in the field of the micro-Doppler effect in bistatic SAR for this configuration. The bistatic geometry considered is shown in Figure 1 where x is the range direvtion and y is the azimuth direction.

At the start of the acquisition (slow time $\eta = 0$) the receiver Rx is located in position $\{0, 0, h_R\}$ while the transmitter Tx is at $\{x_T, y_T, h_T\}$. A point target P in the centre of the illuminated scene is located in position $\{x_P, y_P, 0\}$. The distance in range between the receiver and P is $X_R = x_P$, while the range distance between the transmitter and P is $X_T = x_P - x_T$; the azimuth distance between the receiver

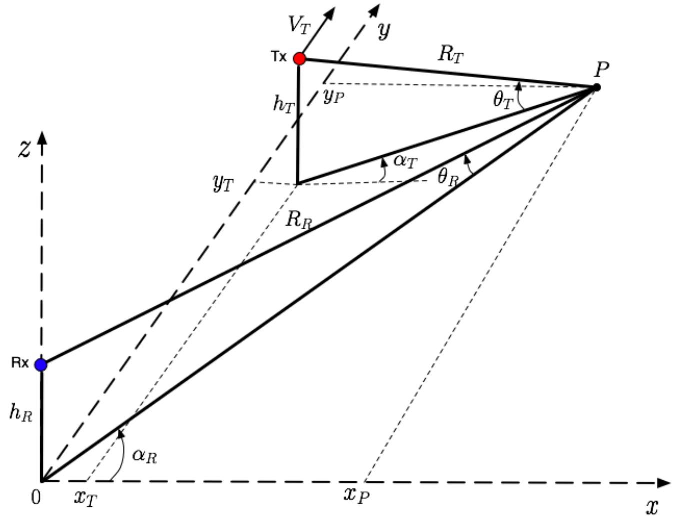

Figure 1: Bistatic SAR geometry with fixed receiver

and P is $Y_R = y_P$, while the azimuth distance at $\eta = 0$ between the transmitter and P is $Y_T = y_P - y_T$. θ_R and θ_T represent the depression angles while α_R and α_T are the squint angle for the receiver and the transmitter respectively. The transmitter is moving with velocity V_T in the y direction, because of the null velocity the receiver slant range is $R_R(\eta) = \sqrt{X_R^2 + Y_R^2 + h_R^2}$ while the transmitter slant range is $R_T(\eta) = \sqrt{X_T^2 + (Y_T - \eta V_T)^2 + h_T^2}$, the bistatic slant range history is the sum of the receiver and transmitter slant range history $R(\eta) = R_T(\eta) + R_R(\eta)$. This is an important factor for the bistatic SAR processing describing the phase history of the received signal.

III. Micro Doppler effect from vibrating target in BSAR

The baseband model of the received bistatic signal from P can be written as [11]:

$$s(\tau,\eta) = A_0 w_r\left(\tau - \frac{R(\eta)}{c}\right) w_{az}(\eta) \exp\left\{-j\frac{2\pi f_0 R(\eta)}{c} + j\pi K_r\left[\tau - \frac{R(\eta)}{c}\right]^2\right\} \quad (1)$$

where τ is the fast time, A_0 is the complex backscatterer coefficient, f_0 is the carrier frequency K_r is the range chirp rate, $w_r(.)$ is the range envelope and $w_{az}(.)$ is the composite antenna pattern of the transmitter and receiver. The micro-Doppler effect of interest generally exhibits a dynamic of the same order as the slow time, for this reason the micro-motions will not have appreciable effects in the fast time and the range compression of (1) can be performed without affecting the analysis. The range compressed signal then results [11]:

$$s_{rc}(\tau,\eta) = p_r\left(\tau - \frac{R(\eta)}{c}\right) w_{az}(\eta) \exp\left\{-j\frac{2\pi f_0 R(\eta)}{c}\right\} \quad (2)$$

where $p_r(\tau)$ is the range envelope that includes the amplitude factor.

The point target P has a micro-motion radial velocity V_v. For our purpose we are assuming that the clutter and a possible constant motion of the target were removed using other processing techniques such as a space-time adaptive processing [12].

With these assumptions the point target P will still have a velocity V_v in the range direction. From Figure 1 the slant range history can be written as:

$$R(\eta) = \sqrt{(X_T - \eta V_v)^2 + (Y_T - \eta V_T)^2 + h_T^2} + \sqrt{(X_R - \eta V_v)^2 + Y_R^2 + h_R^2} = R_T(\eta) + R_R(\eta) \quad (3)$$

The slant range history is directly related to the phase of the received signal in the azimuth direction:

$$\Phi(\eta) = \frac{2\pi R(\eta)}{\lambda_c} \quad (4)$$

where λ_c is the carrier wavelength. From the phase history in (4) the instantaneous frequency can be obtained. However in order to obtain an explicit expression of the different Doppler frequency components a Taylor series approximation of the slant range is applied, where for orders greater than one, the micro motion effect is assumed to be negligible. The receiver slant range become:

$$R_R(\eta) \approx \sqrt{X_R^2 + Y_R^2 + h_R^2} - \frac{\eta V_v X_R}{\sqrt{X_R^2 + Y_R^2 + h_R^2}} = R_{0R} - \frac{\eta V_v X_R}{R_{0R}} \quad (5)$$

While the transmitter slant range can be approximated with:

$$R_T(\eta) \approx \sqrt{X_T^2 + Y_T^2 + h_T^2} - \frac{(V_v X_T + V_T Y_T)\eta}{\sqrt{X_T^2 + Y_T^2 + h_T^2}} + \frac{V_T^2 \eta^2}{2\sqrt{X_T^2 + Y_T^2 + h_T^2}} = R_{0T} - \frac{(V_v X_T + V_T Y_T)\eta}{R_{0T}} - \frac{V_T^2 \eta^2}{2R_{0T}} \quad (6)$$

Using (5) and (6) the slant range history (3) can be written:

$$R(\eta) \approx R_0 - \eta\left(\frac{V_v X_R}{R_{0R}} + \frac{V_v X_T}{R_{0T}} + \frac{V_T Y_T}{R_{0T}}\right) + \frac{V_T^2 \eta^2}{2R_{0T}} \quad (7)$$

where R_{0R} and R_{0T} are the slant ranges for the receiver and the transmitter at the start of the acquisition, and $R_0 = R_{0R} + R_{0T}$. The expression of $R(\eta)$ in (7) can be separated into two components, a bistatic SAR component and a target motion component, $R(\eta) \approx R_{BSAR}(\eta) + R_{Target}(\eta)$ where:

$$R_{BSAR}(\eta) = R_0 - \frac{V_T Y_T}{R_{0T}}\eta + \frac{V_T^2 \eta^2}{2R_{0T}} \quad (8)$$

$$R_{Target}(\eta) = \left(\frac{V_v X_R}{R_{0R}} + \frac{V_v X_T}{R_{0T}}\right)\eta \quad (9)$$

Also the phase history can be divided into two components:

$$\Phi(\eta) = \frac{2\pi R(\eta)}{\lambda_c} \approx \frac{2\pi(R_{BSAR}(\eta) + R_{Target}(\eta))}{\lambda_c} = \\ = \Phi_{BSAR}(\eta) + \Phi_{Target}(\eta) \quad (10)$$

Using the derivative of (10) the istantaneous frequency is obtained as:

$$f_D(\eta) = \frac{1}{2\pi}\frac{d}{d\eta}\Phi(\eta) = \frac{1}{2\pi}\frac{d}{d\eta}\Phi_{BSAR}(\eta) + \frac{1}{2\pi}\frac{d}{d\eta}\Phi_{Target}(\eta) = \\ = \frac{1}{\lambda_c}\frac{d}{d\eta}R_{BSAR}(\eta) + \frac{1}{\lambda_c}\frac{d}{d\eta}R_{Target}(\eta) = \\ = f_{BSAR}(\eta) + f_{MD}(\eta) \quad (11)$$

The instantaneous signal frequency has then two components $f_{BSAR}(\eta)$, a bistatic SAR component and a micro-Doppler component $f_{MD}(\eta)$.
The f_{BSAR} contains the Doppler centroid, the linear and the quadratic modulation term. This component is known from the geometry and does not affect the micro-Doppler frequency. It is not considered further in the analysis.
The explicit form of $f_{MD}(\eta)$ is:

$$f_{MD}(\eta) = -\frac{1}{\lambda_c}\frac{d}{d\eta}\left(\frac{X_R}{R_{0R}} + \frac{X_T}{R_{0T}}\right)V_v\eta \quad (12)$$

Considering a point target P vibrating with a vibration:

$$M(\eta) = A_v cos(w_v\eta) \quad (13)$$

where A_v is the amplitude and w_v is the frequecy of the vibration respectively, then $V_v\eta$ in (12) can be replaced with $M(\eta)$, obtaining:

$$f_{MD}(\eta) = -\frac{1}{\lambda_c}A_v\left(\frac{X_R}{R_{0R}} + \frac{X_T}{R_{0T}}\right)\frac{d}{d\eta}cos(w_v\eta) \\ = \frac{1}{\lambda_c}A_v w_v\left(\frac{X_R}{R_{0R}} + \frac{X_T}{R_{0T}}\right)sin(w_v\eta) \quad (14)$$

Referring to Figure 1 the relations between the slant ranges and the and the angles can be written:

$$R_{GT} = \frac{X_T}{cos(\alpha_T)} = R_{0T}sin(\theta_T) \Rightarrow \frac{X_T}{R_{0T}} = sin(\theta_T)cos(\alpha_T) \quad (15)$$

$$R_{GR} = \frac{X_R}{cos(\alpha_R)} = R_{0R}sin(\theta_R) \Rightarrow \frac{X_R}{R_{0R}} = sin(\theta_R)cos(\alpha_R) \quad (16)$$

Where R_{GT} and R_{GR} are the ground ranges for the transmitter and the receiver respectively. Equation (14) can be written in terms of the squint and depression angles:

$$f_{MD}(\eta) = \frac{1}{\lambda_c}A_v w_v(sin(\theta_R)cos(\alpha_R)+ \\ + sin(\theta_T)cos(\alpha_T))sin(w_v\eta) \quad (17)$$

Equation (17) shows that the micro-Doppler signature depends on the bistatic geometry and is different from the micro-Doppler in the monostatic geometries [8], [9]. A bistatic factor ρ that includes the geometry dependence of the micro-Doppler signature can be defined as:

$$\rho = sin(\theta_R)cos(\alpha_R) + sin(\theta_T)cos(\alpha_T) \quad (18)$$

Then the micro-Doppler frequency becomes:

$$f_{MD}(\eta) = \frac{2\pi}{\lambda_c}A_v w_v \rho sin(w_v\eta) \quad (19)$$

Equation (19) represents the micro-Doppler signature for a bistatic SAR system that is connected to the signature in the monostatic case [9] through the following equation:

$$f_{MD}(\eta) = \frac{f_{MD_{Mono}}(\eta)\rho}{2} \quad (20)$$

From (20) it can be seen that for $\rho = 2$ the bistatic signature is equivalent to the monostatic signature.

A. Effect on the focussing

Using the BSAR configuration given in Table I an example of the slant range history of a vibrating point target compared with a stationary point target is shown in Figure 2. The simulated point target is vibrating with a 10 Hz frequency and a 1 mm amplitude. From Figure 2 the effect of the vibration is evident on the range history for such a small amplitude of the vibration. The phase modulation introduced from the vibration in the signal phase (10) introduces the effect known as paired echoes [13]. The Doppler shift introduced by the vibration creates an infinite number of ghost targets in the focussed image, and as in [13] the received signal may be expanded in a series of Bessel functions of the first kind.

Tx Velocity	75	m/s
X_T	1600	m
X_R	200	m
Y_T	16	m
Y_R	200	m
h_T	1800	m
h_R	100	m
Acquisition time	0.5	s
Vibration amplitude	0.001	m
Vibration frequency	10	Hz

Table I: Simulated bistatic configuration with fixed receiver for the slant range history in Figure 2.

$$J_k(B) = \frac{1}{2\pi}\int_{-\pi}^{\pi} e^{j(Bsinw_v\eta - kw_v\eta)}dw_v\eta \quad (21)$$

where $B = \frac{2\pi}{\lambda_c}A_v(sin(\theta_R)cos(\alpha_R) + sin(\theta_T)cos(\alpha_T))$ and $J_k(B)$ decreases with increasing k. Thus the received signal

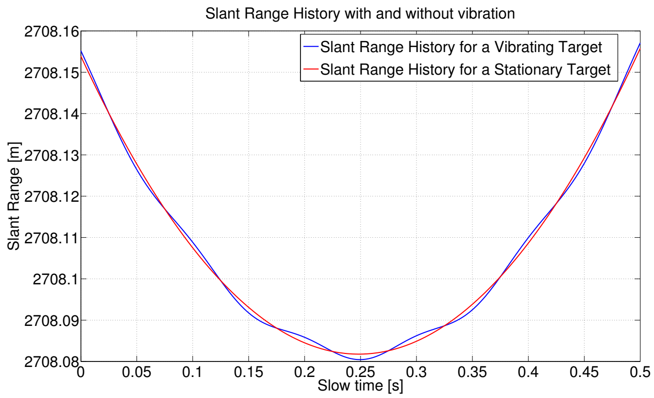

Figure 2: Slant range history for a vibrating target and for a stationary target.

can be written as:

$$
\begin{aligned}
s_{rc}(\tau,\eta) &= p_r\left(\tau - \frac{R(\eta)}{c}\right) w_{az}(\eta) \\
&e^{-j\frac{2\pi f_0 R_{BSAR}(\eta)}{c}} \sum_{k=-\infty}^{\infty} J_k(B) e^{jkw_v\eta} = \\
&p_r\left(\tau - \frac{R(\eta)}{c}\right) w_{az}(\eta) e^{-j\frac{2\pi f_0 R_{BSAR}(\eta)}{c}} \\
&[J_0(B) + J_1(B)e^{jw_v\eta} - J_1(B)e^{-jw_v\eta} \\
&+ J_2(B)e^{j2w_v\eta} + J_2(B)e^{-j2w_v\eta} \\
&+ J_3(B)e^{j3w_v\eta} - J_3(B)e^{-j3w_v\eta} + \cdots]
\end{aligned}
\tag{22}
$$

Unlike [13] the amplitude factor of the ghost scatterers, represented by $J_k(B)$, depends on the bistatic SAR geometry. Thus depending on the particular geometry the effect on the focussed image of a particular vibrating target will be more or less evident.

IV. Simulation Results

Vibrating targets were simulated and the effect on bistatic SAR imaging is analyzed. The result of bistatic focussing for two different configurations with transmitter altitudes of 2100 m and 900 m for a 94 GHz system are shown in Figure 3-a and 3-b respectively. The simulated point target is vibrating at 10 Hz with an amplitude of 0.5 mm. The resulting focussed image in both cases show the presence of ghost scatterers along the azimuth direction on both sides of the point scatterer. However the same vibration exhibits a different number of ghost scatterers with different amplitudes for the two configurations. This aspect can be analyzed and confirmed using the discussion in Section III-A. For the first configuration, Figure 3-a, the bistatic factor is 1.0143 and the value of B in (22) is 0.9984, while in the simulation shown in Figure 3-b the bistatic factor is 1.5382 and $B = 1.5141$. With these values the Bessel functions of the first kind $J_k(B)$ can be computed for both configurations, these values are weighting the amplitude of the scatterer and of the ghost scatterers. The computed values of the first four orders of $J_k(B)$ for the two configurations are shown in Table II. The values of $J_k(B)$ in

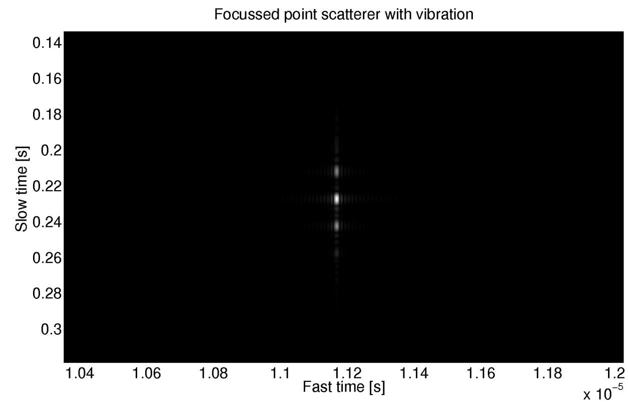

(a)

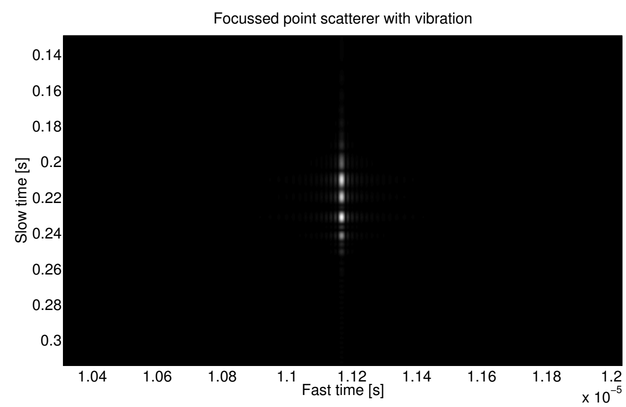

(b)

Figure 3: Focussed point targets in a bistatic SAR system with fixed receiver. The vibrating amplitude is 0.5 mm and the vibration frequency is 10 Hz. In (a) the results are shown for a transmitter at 2100 m of altitude while in (b) the results are shown for the transmitter at 900 m. In (a) the number of visible ghost scatterers is smaller than in (b)

Order of $J_k(B)$	**Config. (a)**	**Config. (b)**
0	0.7659	0.5039
1	0.4395	0.5599
2	0.1146	0.2356
3	0.0195	0.0625

Table II: Computed values of the 1^{st} kind Bessel functions for the two configurations.

Table II confirm that for the configuration simulated in Figure 3-a the amplitude of the real point scatterer is higher than those for the ghost scatterers pairs while for the configuration in Figure 3-b the amplitude of the ghost scatterers is greater than the real point scatterers for the first pair of ghosts.

V. Conclusion

In this paper the micro Doppler effect from vibrating targets in bistatic SAR systems was investigated. The bistatic configuration with a fixed receiver was used to derive an expression for the bistatic micro-Doppler effect. The effect on the focussed image was analysed and simulations to verify the derived model were presented. The bistatic case shows a substantial difference to that of the traditional monostatic case demonstrating that the effect on the focussed image is influenced by the bistatic geometry.

Acknowledgment

This work was supported by the Engineering and Physical Research Council (grant N. EP/H012877/1), the MOD University Defence Research Centre in Signal Processing and Selex-Galileo Edinburgh.

References

[1] M. Cherniakov, *Bistatic Radar: Emerging Technology*. John Wiley, Ltd, 2008.

[2] I. Walterscheid, T. Espeter, A. Brenner, J. Klare, J. Ender, H. Nies, R. Wang, and O. Loffeld, “Bistatic SAR experiments with PAMIR and TerraSAR-x -setup, processing, and image results,” *Geoscience and Remote Sensing, IEEE Transactions on*, vol. 48, no. 8, pp. 3268 –3279, 2010.

[3] M. Zink, G. Krieger, H. Fiedler, I. Hajnsek, A. Moreira, and M. Werner, “Tandem-x - the first bistatic sar formation in space,” *Advanced RF Sensors for Earth Observation (ARSI), ESA/ESTEC, The Netherlands*, 2006.

[4] G.Yates and A. Horne, “Bistatic SAR image formation,” in *Proc. European Conference of Synthetic Aperture Radar,EUSAR’04, Ulm, Germany*.

[5] M. Antoniou, R. Saini, and M. Cherniakov, “Results of a space-surface bistatic SAR image formation algorithm,” *Geoscience and Remote Sensing, IEEE Transactions on*, vol. 45, no. 11, pp. 3359 –3371, 2007.

[6] A. Goh, M. Preiss, N. Stacy, and D. Gray, “Bistatic SAR experiment with the ingara imaging radar,” *Radar, Sonar Navigation, IET*, vol. 4, no. 3, pp. 426 –437, 2010.

[7] S. Duque, P. Lopez-Dekker, and J. Mallorqui, “Single-pass bistatic SAR interferometry using fixed-receiver configurations: Theory and experimental validation,” *Geoscience and Remote Sensing, IEEE Transactions on*, vol. 48, no. 6, pp. 2740 –2749, 2010.

[8] T. Sparr and B. Krane, “Micro-doppler analysis of vibrating targets in SAR,” *Radar, Sonar and Navigation, IEE Proceedings -*, vol. 150, no. 4, pp. 277–83, 2003.

[9] M. Ruegg, E. Meier, and D. Nuesch, “Vibration and rotation in millimeter-wave SAR,” *Geoscience and Remote Sensing, IEEE Transactions on*, vol. 45, no. 2, pp. 293 –304, 2007.

[10] L. Cohen, “Time-frequency distributions-a review,” *Proceedings of the IEEE*, vol. 77, no. 7, pp. 941 –981, Jul. 1989.

[11] Y. L. Neo, “Digital processing algorithms for bistatic synthetic aperture radar data,” Ph.D. dissertation, The University of British Columbia, 2007.

[12] R. Klemm, *Principles of Space-Time Adaptive Processing*, 3rd ed. IET, RADAR, SONAR, NAVIGATION AND AVIONICS SERIES 21, 2006.

[13] V. Chen, F. Li, S.-S. Ho, and H. Wechsler, “Micro-doppler effect in radar: phenomenon, model, and simulation study,” *Aerospace and Electronic Systems, IEEE Transactions on*, vol. 42, no. 1, pp. 2 – 21, 2006.